Supplementary Materials for

Striatal dopamine mediates hallucination-like perception in mice

K. Schmack*, M. Bosc, T. Ott, J. F. Sturgill, A. Kepecs*

*Corresponding author. Email: schmack@cshl.edu (K.S.); akepecs@wustl.edu (A.K.)

Published 2 April 2021, *Science* **372**, eabf4740 (2021)
DOI: 10.1126/science.abf4740

This PDF file includes:

Other supplementary material for this manuscript includes:

Data S1 (zipped folder)

Materials and Methods

Mice

A total of 24 mice (14 female) were used for the study. For behavioral and photometry experiments, wild-type C57BL/6J were purchased from Jackson Laboratory, Bar Harbor, ME. For optogenetics experiments, transgenic DAT-Ai32 C57BL/6J mice were generated in-house by breeding DAT::Cre homozygous mice with Ai32 homozygous mice. Mice were minimum 10 weeks of age at the beginning of the training, and between 15 and 50 weeks of age during data collection. See Table S1 for details on the age ranges in the different experiments. Food was available ad libitum, and mice had scheduled access to water with daily body weight monitoring to ensure that their body weight remained above 85% of the initial weight. Mice received water during behavioral sessions. All procedures involving animals were carried out in accordance with National Institutes of Health standards and were approved by the Cold Spring Harbor Laboratory Institutional Animal Care and Use Committee.

Behavioral Setup

Behavioral testing was conducted in sound-isolated, ventilated chambers. The behavioral setup consisted of three ports equipped with waterspouts for reward delivery, infrared photodiodes for detecting port entry and LED diodes for light signals. Water rewards were delivered from gravity-fed reservoirs regulated by solenoid valves. Auditory stimuli were presented using generic speakers that were calibrated prior to the experiments to ensure standardized sound pressure levels. Stimulus presentation and reward delivery was controlled using a Windows computer and an ASUS® Xonar DX soundcard and the open-source behavioral controller Bpod 1.0 with custom software written in MATLAB.

Auditory detection task with time-investment-based confidence reports

Hallucination-like perceptions (HALIPs) in mice were quantified in an auditory detection task with time-investment based confidence reports. During the entire experiment, constant auditory white background noise (40 dB SPL) was playing. Mice self-initiated a trial by poking into the center port. After a variable interval between 0.1 s and 0.5 s (exponential distribution with decay constant of 0.2 s), the center port lit up for 0.1 s. On signal trials, the center port light cue was accompanied by a simultaneous upsweep tone signal (10 – 15 kHz) with varying volume between 35 dB SPL and 65 dB SPL on top of the background noise. On no-signal trials, the center port light cue was not accompanied by any additional signal. Signal and no-signal trials were randomly interleaved in equal proportions.

After stimulus delivery, mice responded by withdrawing from the center port and moved to the left or right choice port. Reward was available at one (e.g. the left) port on signal trials and at the other (e.g., the right) port on no-signal trials. The stimulus–reward mapping was pseudorandomized across animals. For correct choices, reward was delivered after a variable delay between 0.5 s and 5 s. The reward delay was drawn from an exponential distribution with decay constant of 1 s resulting in a relatively constant level of reward expectancy over a range of delays. In a small fraction of correct choices (5% of trials) rewards were omitted. These reward omission trials allowed us to measure the time the mice were willing to invest on correct trials (without ending the

time investment period by external reward delivery). For incorrect choices, no reward and no feedback was delivered thereby enabling us to measure time investment at each incorrect trial.

Signal volumes were continuously varying and uniformly distributed in the range 35dB to 65 dB SPL with one exception: In a sub-group of mice (N=4) during the initial behavioral testing (Fig. 1, S01, S03), signal volumes were set at discrete levels (e.g. 35dB, 50dB, and 65dB SPL). Behavioral performance was comparable between mice presented with continuous range of signal volumes and those presented with discrete signal volume levels (**Fig. S03A-B**).

To perform the task described above, mice went through a multistep training procedure typically lasting 6–16 weeks gradually introducing more difficult stimuli, longer reward delays and reward omission trials. The training procedure consisted of three stages.

(I) Coarse discrimination. In this training stage, mice were trained to discriminate between the two different categories of stimuli (no signal vs signal). To this end, we used noise only stimuli and loud signals (65dB SPL) embedded in noise (40dB SPL). As soon as animals started to discriminate between these two stimuli (accuracy >60% over three sessions), we proceeded to the second training stage.

(II) Fine discrimination. We continued to train the animals with the same two categories of stimuli (no signal vs signal) but increased the discrimination difficulty by broadening the range of used signal volumes (between 35 dB and 65dB SPL). Animals were trained with these stimuli until their psychometric curves appeared stable across several sessions.

(III) Feedback delay. We then increased the reward delay defined as the time between the mouse poking into the correct choice port and reward delivery. Increases were performed gradually over one to three sessions until the final feedback delay distribution was reached. After stable performance was reached (accuracy>70% over several sessions), we introduced catch trials by omitting the reward on 5% of the trials.

Animals' performance increased over the course of the training and did not decrease when transitioning form one training stage to the next one (**Fig. S01**).

Behavioral data analysis

Behavioral data from mice and humans was analyzed using custom Matlab code. We excluded the 20 first trials of each session because these were easy trials aimed at re-habituating mice to the task. To ensure the quality of the behavioral data, we excluded sessions with an accuracy below 70% (6.8% of sessions) and trials with very short time investments < 2s (1.1% of trials).

We fitted a psychometric function to explain the percentage of signal choices as a function of the stimulus SNR. SNR was calculated as the signal volume in dB SPL minus the noise volume in dB SPL. Note that on no-signal trials the SNR is arbitrary because signal volume is not defined on these trials. We dealt with this arbitrary SNR on no-signal trials in two different ways. First, for fitting psychometric curves for display, we followed the standard approach for the psychophysical treatment of detection tasks: we fitted a three-parameter psychometric function that included an asymptotic guess or false alarm rate. We set the SNR on no-signal trials to -40 dB SPL and fitted

the psychometric function: $p(\vartheta = signal \,|\, \mu_L) = \gamma + (1-\gamma) * \Phi(\mu_L; b, \sigma_L)$. Here, ϑ is the choice and μ_L is the SNR of the stimulus. Φ is a cumulative Gaussian distribution function mean b and standard deviation σ_L. The parameter b denotes the decision boundary, while the parameter σ_L specifies the level of sensory noise. The inclusion of a guess rate γ renders the exact value of the SNR on no-signal trials irrelevant (as long as it is sufficiently low), because it allows to estimate choices on no-signal trials independently of the signal trials. Second, for all other analyses, we used signal trials only to fit the two-parameter psychometric function $p(\vartheta = signal \,|\, \mu_L) = \Phi(\mu_L; b, \sigma_L)$ and set the SNR on no-signal trials to the value that was expected from the observed false alarm rate (i.e. the inverse of a cumulative normal distribution with the mean b and standard deviation σ_L). This procedure allows the derivation of statistical decision confidence and belief-updates without additional assumptions about how confidence behaves on guesses.

Statistical decision confidence c was derived as previously described (*4-8*): $c = P(\vartheta = correct \,|\, \vartheta, x)$. Here, ϑ is the choice and x is the internal estimate of the stimulus or percept, because the observer does not have direct access to the stimulus. This percept x is given by sampling from a normal distribution centered around the SNR μ_L with standard deviation σ_L. The choice ϑ is then determined by whether the percept lies to the left or the right of the decision boundary b, and the probability that ϑ is correct can be calculated using a Monte Carlo simulation (*8*).

To derive statistical confidence for each subject, we first fitted the subject's psychometric choice behavior with the two-parameter psychometric function described above (**Fig. S3A**). This provided us with individual parameter estimates for σ_L and b, that we then used to simulate percepts, choices and outcomes 100 times for each of the experimental SNRs μ_L. Simulated percepts were then grouped into 200 bins spanning the range of percepts, and the fraction of trials with correct outcomes in each percept bin was taken as the confidence associated with all the simulated percepts in this bin. To transform simulated confidence values (by definition probability estimates between 0.5 and 1) into time investments (above 2 seconds), we used parameter-free quantile normalization as previously described (*5*, **Fig. S3B**).

We assessed whether time investments follow statistical confidence in two different ways: (i) via the *qualitative shape* of three previously described signatures and (ii) via the *quantitative fit* of the no-free parameter statistical confidence model. For *qualitative* visualization of the similarity between time investments and statistical confidence, we plotted the predicted time investment together with the observed time investment in previously described signatures (**Fig. S3C**). To *quantify* how well statistical confidence explained time investment behavior, we calculated the correlation between these two measures binned according to SNR and outcome (**Fig. S3D**). As a control, we repeated the entire procedure 1000 times on shuffled data, by randomly shuffling model-derived confidence values. To remove between-session variance in time-investments for modeling purposes, each time investment was normalized by subtracting the session mean and adding the grand mean (Cosineau method).

Crucially, statistical confidence predictions are not fits to the time investment behavior but rather no free parameter computations based on the psychometric choice behavior. Consequently, subtle differences in the psychometric choice behavior (e.g. due to individual variability or due to experimental conditions) are associated with non-trivial changes in the predicted statistical confidence (**Fig. S02B-E**). This central characteristic of statistical confidence has two important implications.

1. Plots of statistical confidence in the three signatures (e.g., Fig. 1C-E) are different from classic psychometric plots (e.g. Fig. 1B) because they are predictions and not fits.

2. Time investments can only be compared to the respective, quantitative confidence predictions generated for a particular individual or experimental condition. This means that time investments themselves should not be averaged or compared across different individuals or experimental conditions. Instead, some quantitative measure for the fit (e.g. correlation, see above) between time investments and the respective statistical confidence predictions can be used for such averaging or comparisons.

To assess the effect of experimental interventions (induction of signal expectations, ketamine administration, optogenetics stimulation, reversal of optogenetics stimulation by haloperidol administration) on HALIPs, we conducted repeated-measures ANOVAs on false alarm rates, time-investment based confidence in false alarms and the squared correlation coefficients between statistical confidence predictions and time investments (see above). We used the MATLAB *fitrm*, *ranova* and *multcompare* functions with default settings. Tukey's honest significant difference criterion was used to correct for multiple comparisons in post-hoc pair-wise comparisons. To remove between-subject variance for plotting purposes, each observation was normalized by subtracting the subject mean and adding the grand mean (Cosineau method).

In the third panel of the summary figure, we show three data points from two different cohorts next to each other (cohort 1 laser on, cohort 1 laser off, cohort 2 laser on + haloperidol). For simplicity, we report the p-values from two non-parametric Wilcoxon's signed rank tests comparing data points within each cohort (cohort 1 laser on vs laser off, cohort 2 laser on + haloperidol vs laser on + vehicle),

Drug administration

For the ketamine manipulation, mice received intraperitoneal injections of ketamine or saline (0.1-0.3 ml, 30mg/kg diluted in 0.9% saline or 0.9% saline alone) immediately before placed into the behavioral box. Mice usually then showed some transient agitation with stereotypical movements (running in circles) and then started task performance on their own pace, which took typically ~15 minutes. For the haloperidol rescue of the optogenetics manipulation (see below), mice received 10-20 µl subcutaneous injections of haloperidol 0.15mg/kg diluted in dimethyl sulfoxide or dimethyl sulfoxide only 30 minutes prior to the experiment via a microliter syringe (Hamilton Gastight 1700).

Human online experiment

Human participants were recruited via the crowdsourcing service Amazon Mechanical Turk. Participants performed a computerized version of the auditory detection task with confidence reports. Very similar to the mouse version, a constant auditory background noise (10 digital units) was

playing during the entire experiment, and participants self-initiated trials with the arrow-down key on their keyboard. After a variable interval of between 0.1 s and 0.5 s (exponential distribution with decay constant of 0.2s), a loudspeaker signal changed color for .5s. On signal trials, this visual cue was accompanied by a simultaneous upsweep tone signal (0.1 – 0.2 kHz) with varying volume between 0 and 10 digital units (uniform distribution) on top of the background noise. On no-signal trials, the visual cue was not accompanied by any additional signal. Signal and no-signal trials were randomly interspersed at equal proportions.

After stimulus delivery, participants responded by pressing the right or the left arrow key to indicate whether they had perceived a signal or not. To control for side biases, the stimulus-response mappings were randomized across participants. After indicating their perception, participants rated their confidence in their choice by positioning a slider on a continuous vertical visual scale. After this, feedback was delivered: for correct choices, 1000 points were added to the score, for error choices the score remained unchanged.

Prior to the auditory detection task, participants performed a headphone screening (*28*). This is a brief psychophysical test that exploits the phenomenon of phase cancellation for determining whether online experiment participants are wearing headphones.

After the auditory detection task, participants completed questionnaires to quantify hallucinations and other psychopathological symptoms. We used the freely available Cardiff Anomalous Perception Scale (*12*), an instrument that is designed to measure hallucination-like experiences in non-clinical samples. Moreover, we used the commercial Symptom Checklist 90 – Revised (Pearson Clinical ®), an instrument that measures a wide array of psychopathological symptoms along several dimensions.

The task and questionnaires were programed in Javascript using the React library, and executed on a website. A total of n=2276 completed a brief screening that consisted of 100 trials of the auditory detection task. Out of these, n=568 participants were selected based on predefined quality control criteria (accuracy>70% and miss rate on easy trials <10%, confidence ratings spanning a minimum of 5% of the visual scale), and re-invited for participation in the experiment. Out of these, n=359 came back to complete the experiment. From these, n=139 participants were excluded when applying our quality control criteria to the full dataset (n=5 accuracy<70% or miss rate on easy trials >10%, n=29 confidence ratings < 5% span, n=105 both). This left us with a sample of n=220 participants (see **Table S2** for demographic information). Participants completed a median of 454 trials (range 276 to 770), depending on how many sessions they were willing to complete. They were paid $8 dollars/hour. All human experiments were conducted according to the Declaration of Helsinki, and were approved by the Cold Spring Harbor Laboratory Institutional Review Board.

Behavioral data from human participants were analyzed analogously to the mouse experiments. Psychometric curves and statistical decision confidence were derived by the procedures described above. Here, SNR was given by the difference between the signal and the noise volume (in digital units as specified in the Javascript code). Confidence ratings were given by the position of the confidence slider in pixels and were rescaled to values between 0 and 1 to correct for individual variability in how far participants spread their ratings across the scale. To relate task behavior to the highly skewed questionnaire scores, we used non-parametric Spearman rank correlations. For

visualization purposes only, we plot the fits and standard errors of a robust regression model using the Matlab routines *fitlm* and *predict*. Moreover, in Fig. 2I we do not show data from N=6 participants who showed extreme high-confidence false alarm rates (>75th prctile plus 5 interquartile distances). Inclusion or exclusion of these participants did not affect statistical results. To identify which psychopathological subscales predicted task behavior best, we rank-transformed the data and used a stepwise regression as implemented by the Matlab routine *stepwiselm* with the default forward selection criterion 'SSE' and $p<0.05$.

All procedures involving human participants were approved by the Cold Spring Harbor Laboratory Institutional Review Board. Informed consent was obtained from all participants.

Computational model of belief-updating

To formalize HALIPs in terms of prediction errors and prior expectations, we devised a belief-updating model that uses prediction-error guided updating of prior expectations and combines these prior expectations with the current input by Bayesian inference. In our task, the observer never fully knows the state of the trial but has to actively infer whether a signal is present or not from the current stimulus. In the Bayesian view, the observer's belief about the presence of a signal given the current stimulus can be expressed as a probability distribution:

$$p(signal \mid stimulus) \propto p(stimulus \mid signal) \times p(signal) \tag{1}$$

Here, $p(stimulus \mid signal)$ is the likelihood of a signal that is determined by the current stimulus strength. In line with standard psychophysical treatments of sensory noise, we assume that the likelihood of a signal normally distributed around the SNR of the stimulus with constant variance:

$$p(stimulus \mid signal) = \mathcal{N}(\mu_L, \sigma_L) \tag{2}$$

For simplicity, we further assume that the prior belief about the signal $p(signal)$ is also normally distributed with the distribution:

$$p(signal) = \mathcal{N}(\mu_P, \sigma_P) \tag{3}$$

As a result, the resulting posterior belief about the signal $p(signal \mid stimulus)$ will be also normally distributed:

$$p(signal \mid stimulus) = \mathcal{N}(\mu, \sigma) \tag{4}$$

with

$$\mu = \mu_L + \mu_P \tag{5}$$

and

$$\sigma = \sqrt{\sigma_L^2 + \sigma_P^2} \tag{6}$$

The model assumes that on each trial, the observer samples from this posterior distribution a percept x that represents the observer's estimate of the presence of a signal. The choice ϑ is given by where the percept x lies in relation to a decision boundary b

$$\vartheta = \begin{cases} signal & \text{if x} > b \\ noise & \text{if x} < b \end{cases} \tag{7}$$

The absolute value of the percept x further provides an estimate of the probability that a signal will be present, the signal certainty χ. Given that the percepts x are distributed with $\mathcal{N}(\mu, \sigma)$, and the percept x provides the internal estimate of μ, this signal certainty is given by the cumulative normal distribution Φ with the mean b and standard deviation σ, or

$$\chi(x) = \Phi(x; b, \sigma) \tag{8}$$

Keeping with our definition of confidence as the probability of being correct, signal certainty χ is directly related to the statistical decision confidence c by

$$c = \begin{cases} \chi = \Phi(x; b, \sigma) & \text{if x} > b \\ 1 - \chi = 1 - \Phi(x; b, \sigma) & \text{if x} < b \end{cases} \tag{9}$$[1]

This is the case because the choice depends on whether x is larger or smaller than the decision boundary. If $x > b$, then a signal choice is made and the probability of this signal choice being correct c is equal to the probability of a signal being correct χ. In contrast, if $x < b$, a no-signal choice is made and the probability of this no-signal choice being correct c is one minus the probability of the signal choice being correct, or $1 - \chi$.

After the observer has made a choice with a given confidence, there will be feedback F about whether a signal was truly present, and this will generate a perceptual prediction error δ that updates the mean of the prior belief prior belief μ_P:

$$F = \begin{cases} 1 & \text{if signal observed} \\ 0 & \text{if no signal observed} \end{cases} \tag{10}$$

$$\delta = F - \chi \tag{11}$$

$$\mu_P^{t+1} = \mu_P^t + \alpha\delta \tag{12}$$

where α is a fixed learning rate that is bounded to positive values. Because signal certainty χ is scaled between 0 and 1, the sign of the prediction error δ is positive when the true stimulus was

[1] This notation is equivalent to previous notations using the error function (*5, 6*), because by definition $\Phi(x; b, \sigma) = \frac{1}{2}\left[1 + erf\left(\frac{x-b}{\sigma\sqrt{2}}\right)\right]$.

a signal and negative when the true stimulus was no-signal. Hence, the prior expectation will shift in the direction of the true stimulus, and the size of this shift will depend on how unexpected the stimulus was.

We here assume that the observer will deduce the presence of signal from both rewarded signal choices and non-rewarded no-signal choices, but note that in principle the observer could also learn only from rewarded or non-rewarded choices with the effect of slower learning. For the sake of convenience, we further assume that only the mean of the prior is updated, while the variance of the prior remains constant. This assumption makes the prior mean μ_P directly interpretable as a momentary shift on the decision boundary b, because it has a simple additive effect on the posterior mean μ.

We can further simplify our model by assuming a decision boundary $b = 0$. This is the case because through learning the observer should converge to a level of minimal perceptual surprise. Hence, under stationary conditions, i.e. once the observer has reached a stable level of performance, the prior mean μ_P converges to an average value that is equal to the optimal shift of the boundary b to minimize prediction errors (see **Fig. S3** for an empirical validation of this claim). Therefore, the exact value of the boundary b becomes irrelevant, because it will be shifted to the optimal decision value by the prior mean μ_P. When the decision boundary is set $b = 0$, the average prior mean μ_P can therefore be interpreted as the decision boundary that is optimal with respect to the average stimulus.

μ_P provides a direct quantitative trial-by-trial estimate of the perceptual expectation about whether a signal will be present or not. At the same time, $|\mu_P|$, or the distance of μ_P from the optimal decision boundary, can be interpreted as the expectation of whether a reward will be delivered or not. This is the case because both correct signal choices and correct no-signal rejections yield the same amount of reward, and hence very high signal expectations and very high no-signal expectations (i.e. very low signal expectations) are equivalent to high reward expectations. In this context, both μ_P and $|\mu_P|$ can provide an algorithmic explanation for how dopamine leads to HALIP.

Importantly, the model makes two distinct predictions for how dopamine produces HALIPs. If dopamine encodes expectations about whether a reward will be received, excessive dopamine will be reflected in increased values of $|\mu_P|$ that shift the posterior away from the average stimulus. As a result, perceptual discrimination is impaired with increased error choices and error confidence for both no-signal and signal stimuli. This accounts for overconfident false alarms, i.e. HALIPs, accompanied by increased misses (**Fig. 4K**, middle panel). If, in contrast, dopamine relates to perceptual expectations about whether a signal will be present, excessive dopamine will be reflected in increased μ_P that shift the posterior towards signal perception. As a result, perceptual detection will be biased towards perceiving signals with increased signal choices and signal confidence on both no-signal and signal stimuli. This again accounts for overconfident false alarms, i.e. HALIPs, accompanied by increased hits (**Fig. 4K**, right panel).

To simulate choice and confidence behavior in our auditory detection task with our model, we used the sequences of stimulus SNRs as presented to the mice. The parameters were fixed with the learning rate set to $\alpha = 10$ and the posterior variance set to $\sigma = 17.7$. Note that α is scaled with respect to the stimulus units, i.e. $\alpha = 10$ means that a completely unexpected signal would move the prior mean +10 stimulus units (e.g. dB SPL). Further note that we could use a fixed σ because we assumed both σ_P and σ_L to be fixed. The initial value of μ_P was set to -100 to demonstrate the convergence (**Fig. 4B**), to 0 for all other simulations. We allowed the model to settle on a stable μ_P by running an initial simulation run that was excluded from analysis, before running a total of 10 simulation runs.

Photometry experiment

After mice were fully trained, we injected virus and implanted fibers into VS (ML -1.25mm, AP +1.0mm DV -3.85mm) and TS (ML +3.25mm, AP -1.0mm, DV -2.5mm) under general anesthesia (1-2% isoflurane). Because stimulus-response mapping was randomized across animals, we always chose the right hemisphere for VS injection and implantation and the left hemisphere for TS injection and implantation. To express the dopamine sensor, wild type mice were injected with AAV9-hSyn-DA4.3, an improved variant of a recently described green-fluorescent dopamine sensor $GRAB_{DA}$ (19). As a control, we simultaneously injected AAV1.CAG.tdTomato.WPRE.SV40 (Addgene 105554-AAV1) to express the red-fluorescent protein TdTomato (see below for details).

Injection sites were -0.4 mm and -0.2mm below the fiber implantation site to maximize the signal at the fiber tip. Optical fibers (400 μm core diameter, 0.48 NA) were implanted at the injection sites using the coordinates above. After a post-operative recovery period of 2 weeks, mice were retrained to pre-surgery performance before recording started. Histology after the experiment confirmed successful fiber positioning in all but two recording sites, and these recording sites were therefore excluded from analyses. Two recording sites were excluded because there were no discernible $GRAB_{DA}$ transients. No other recording sites were excluded. See **Fig. S12A-D** for examples and a summary of the fiber implantation sites.

We used a custom dual-color fiber photometry acquisition setup to record simultaneously dopamine activity from green-fluorescent $GRAB_{DA}$ and control signals from red-fluorescent TdTomato. The excitation beam for the green channel was produced by a 470nm LED light source (M470F1 Thorlabs) was collimated via an aspheric lens (F240FC-A Thorlabs), passed through an excitation filter (ET470/24M Chroma), bounced off a dichroic mirror (T495LPXR Chroma). The excitation beam for the red channel was produced by a 565nm LED light source (M656F3 Thorlabs), collimated via an aspheric lens (F240FC-A Thorlabs), passed through an excitation filter ET569/25X and passed through the same dichroic mirror (T495LPXR Chroma). The merged excitation beams were then bounced by another dichroic mirror (59022bs Chroma) and launched into a 400μm core, 0.48NA fiber patch cable using an aspheric lens (F240FC-A Thorlabs). Fluorescence excitation and detection were both accomplished through one multimode optical fiber that was connected to the animal via a fiber-optic rotary joint (FRJ_1x1_FC-FC Doric). Fluorescence emitted from both the green and the red channel was passed through the same dichroic mirror (59022bs Chroma) and split into two separate emission beams by another dichroic mirror (T570LPXR Chroma). Separately, the emission beams were passed through emission filter

(ET525/50M Chroma and ET630/75M, respectively), focused with aspheric condenser lenses (ACL25416U-A Thorlabs), and collected using amplified photodiodes (Newport 2151). To ensure the proper separation of the green and the red channel, the fluorescence signals was amplitude-modulated by sinusoidally varying the command voltage of the LED driver (LEDD1B Thorlabs) with two different frequencies (531 Hz and 211 Hz) and demodulated prior to data processing. Photometry data were acquired using a data acquisition card (PCIe-6321 National Instruments) and synchronized with the behavioral task using Bpod and custom software written in MATLAB (Mathworks).

Fluorescence signals were expressed as the relative fluorescence $dFF = \Delta F / F_0 = (F - F_0) / F_0$. Often F_0 is given by the fluorescence signal during a certain time period that is assumed to be irrelevant, such as the second before the task event of interest. While this approach is perfectly suited for comparing phasic responses to events of interest, it might obfuscate more sustained differences preceding events of interest. For these reasons, we here devised an unconstrained approach that does not rely on temporal assumptions and calculates F_0 as the median-filtered raw signal (window 60s). Hence, dFF represents the fluorescence relative to the surrounding minute, regardless of any task events.

The fluorescence of $GRAB_{DA}$ depends on dopamine, but the photometry signal might also show dopamine-independent fluctuations, e.g. due to movement. To carefully control for this possibility, we simultaneously recorded tdTomato fluorescence. The fluorescence of TdTomato is independent of dopamine, and therefore shows only dopamine-independent fluctuations, e.g. due to movement. TdTomato and $GRAB_{DA}$ signals were both processed as described above, yielding dFF_{RED} and dFF_{GREEN}. Visual inspection of these traces indicated that TdTomato did not reveal tonic and phasic modulations as $GRAB_{DA}$ signals, suggesting that the striatal dopamine signals that we had observed could not be explained by non-dopamine-related fluctuations, e.g. due to movement (**Fig. S8**).

In addition to this qualitative control, we aimed to quantitatively control for ongoing dopamine-independent fluorescence fluctuations. To this end, we corrected the $GRAB_{DA}$ traces by subtracting the variance that is shared between TdTomato and $GRAB_{DA}$ traces. The shared variance provides a quantitative estimate of dopamine-independent fluorescence fluctuations such as movement artifacts, because any factors other than dopamine are expected to affect TdTomato and $GRAB_{DA}$ alike. Similar to previous work (*39*), we used dFF_{RED} to fit a robust regression on $dFF_{GREEN} = a * dFF_{RED}$. The corrected signal was then given by $dFF_{GREEN\_CORRECTED} = dFF_{GREEN} - a * dFF_{RED}$. To ensure that we only included sessions where the TdTomato signal was a meaningful estimate of the non-dopamine-related signal fluctuations, we excluded sessions where the p-value for the regression coefficient a was $p > 0.001$, resulting in the exclusion of 29 out of 169 sessions. Potential reasons for insufficient quality of TdTomato signals on these 29 excluded sessions were equipment malfunction, excessive TdTomato fluorescence saturating the photodetector or insufficient TdTomato fluorescence due to photobleaching.

To quantify tonic baseline dopamine signals and relate them to HALIPs, we integrated the corrected fluorescence traces $dFF_{GREEN\_CORRECTED}$ over a 0.5 s interval before the time-point the mice initiated a trial. We selected 0.5s interval because this was the minimum inter-trial interval and therefore ensured that we had complete data for all trials. Considering a longer time interval of 1s did not produce substantially different findings, which is consistent with our observation that sustained dopamine signals that differentiated between upcoming perceptual choices up to 5s prior to the stimulus (**Fig. S8A-B**). These baseline measures were z-score transformed within each mouse and compared between false alarms and correct rejections as well as between high-confident and low-confident false alarms with paired t-tests.

Optogenetics experiment

After DAT-Ai32 mice were fully trained, we implanted fibers into TS (ML +/-3.25mm, AP -1.0mm, DV -2.5mm) under general anesthesia (1-2% isoflurane). Four animals received bilateral fiber implants, while four animals received unilateral fiber implants in the left hemisphere. In order to control for movement-related, perception-independent effects of unilateral stimulation, two animals that received unilateral fiber implants had one stimulus-response mapping ('left-signal'), while the other two animals with unilateral implants had the opposite stimulus-response mapping ('right-signal'). Optical fibers (200 μm core diameter, 0.39 NA) delivered 0.5mW of 473nm laser light (measured in continuous mode at the fiber tip). During behavioral testing, optical stimulation was performed with 4ms pulses at 2Hz during stimulation blocks (50 trials) interleaved by blocks without stimulation (150 to 250 trials). Stimulation with comparable parameters has been shown to elicit dopamine release in DAT-Ai32 mice both in-vitro (*40*) and in-vivo (*41*). Histology after the experiment confirmed successful fiber positioning in all stimulation sites, and hence no mice were excluded from this data set. See **Fig. S12C** for an example and a summary of the fiber implantation sites.

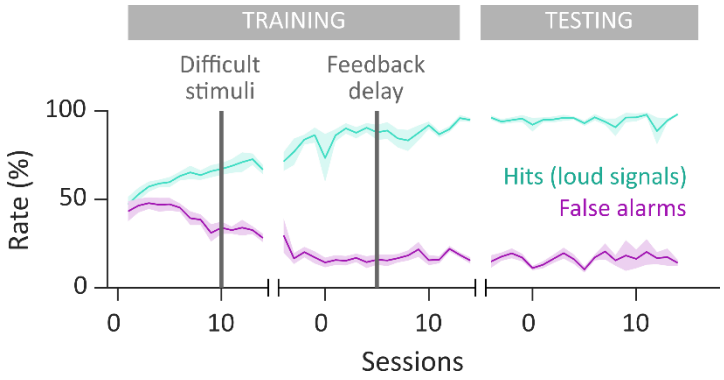

Fig. S1: **Mice learn to discriminate signals from background noise through training.** Hit rates increase and false alarm rates [mean ± SD across mice] decrease throughout training and are stable during testing. In the beginning of the training, mice are only presented with no-signal and very loud signal trials. When mice start to discriminate between these two (accuracy>60%), more difficult stimuli are introduced. When mice reliably discriminate between the two (accuracy>70%), the water reward is delayed for an unpredictable interval and omitted on 5% of the trials. Experimental data is collected during stable performance.

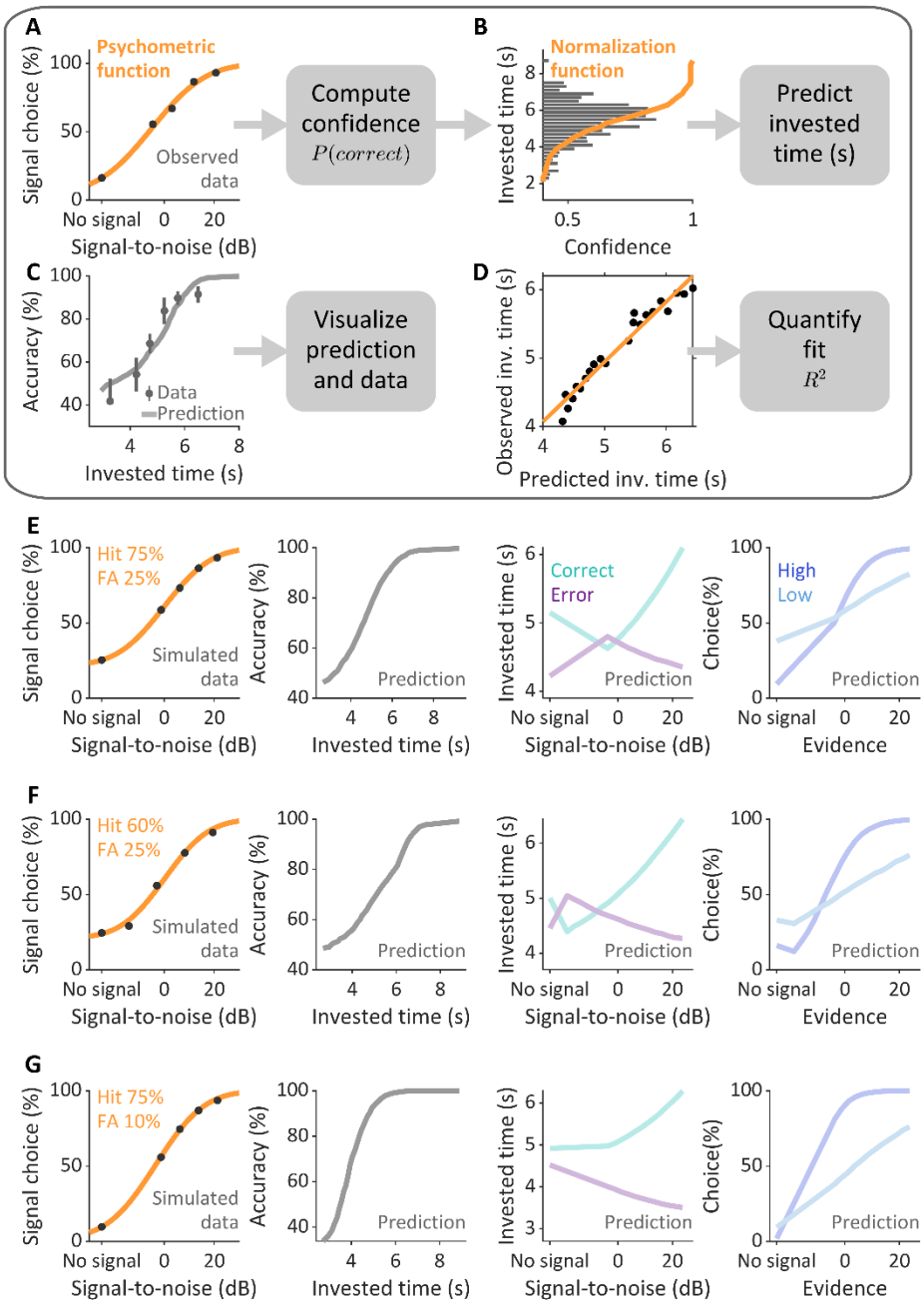

Fig. S2: Statistical confidence is derived from psychometric choice behavior. (A) A subject's choice data is fit with a psychometric function. The resulting parameters are used to simulate percepts, choices and outcomes. This enables computing confidence as the probability being correct given a choice and a percept. (B) Simulated confidence is transformed into predicted invested time by parameter-free quantile normalization. (C) For qualitative comparison of statistical confidence and observed time investment behavior, predicted and observed invested times are plotted together in three signature ways (only one shown here). (D) A quantitative measure of how well statistical confidence explains time investment behavior is calculated by correlating predicted and observed invested times. The resulting squared correlation coefficient R^2 quantifies the degree of variance in the time investment behavior that is explained by statistical confidence.

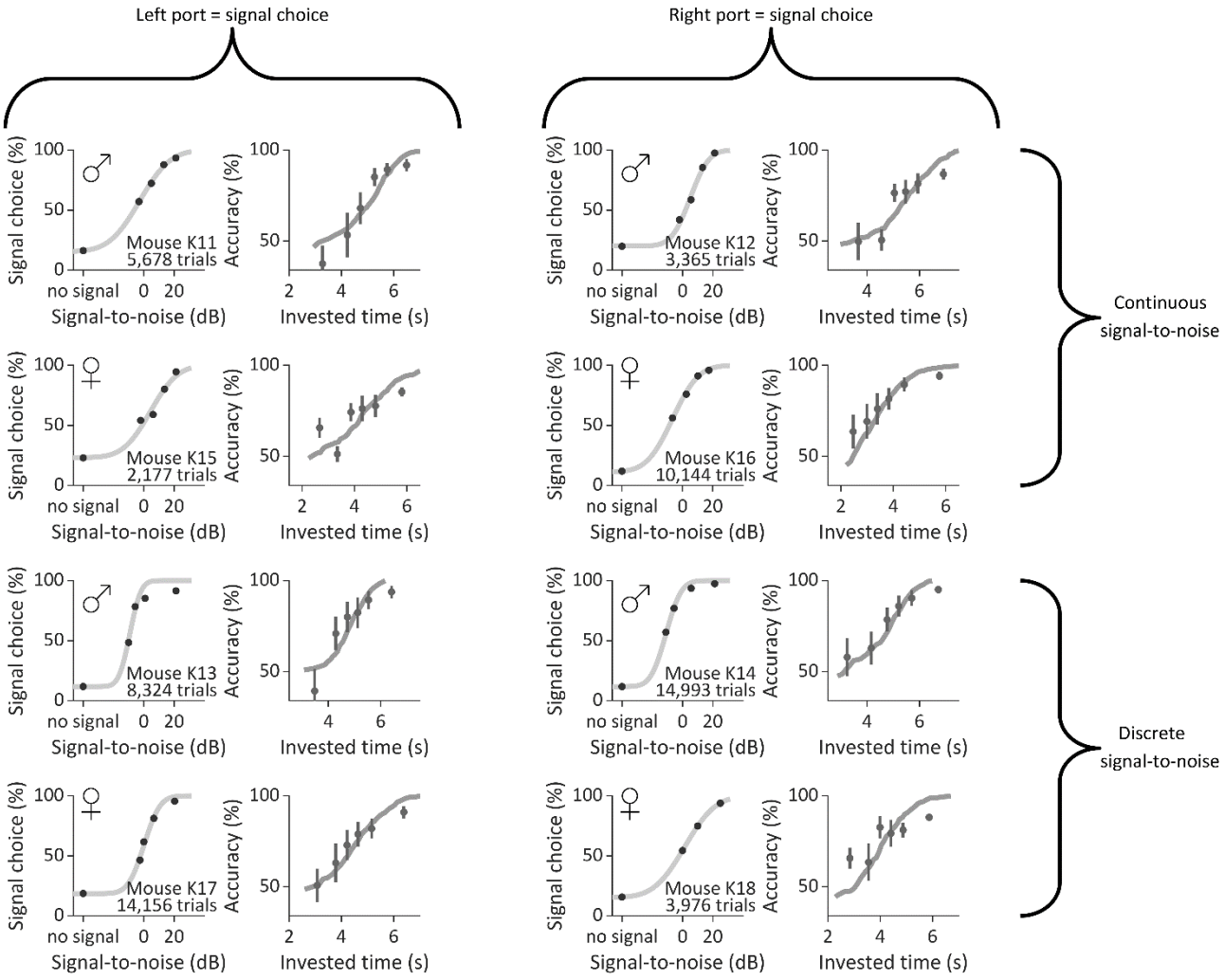

Fig. S3. Psychometric choice and time investment behavior is consistent across mice. All mice show comparable psychometric choice behavior [data pooled across sessions] with substantial false alarm rates on no-signal trials and negligible lapse rates on the loudest signal trials. This is observed regardless of whether mice used the left or the right port to report a signal, suggesting that false alarms cannot be explained by motor biases. This is further observed regardless of whether signal-to-noise ratio was varied continuously or in discrete steps and for both female and male mice. In all mice time, investment behavior [mean ± SD across session] closely follows statistical decision confidence.

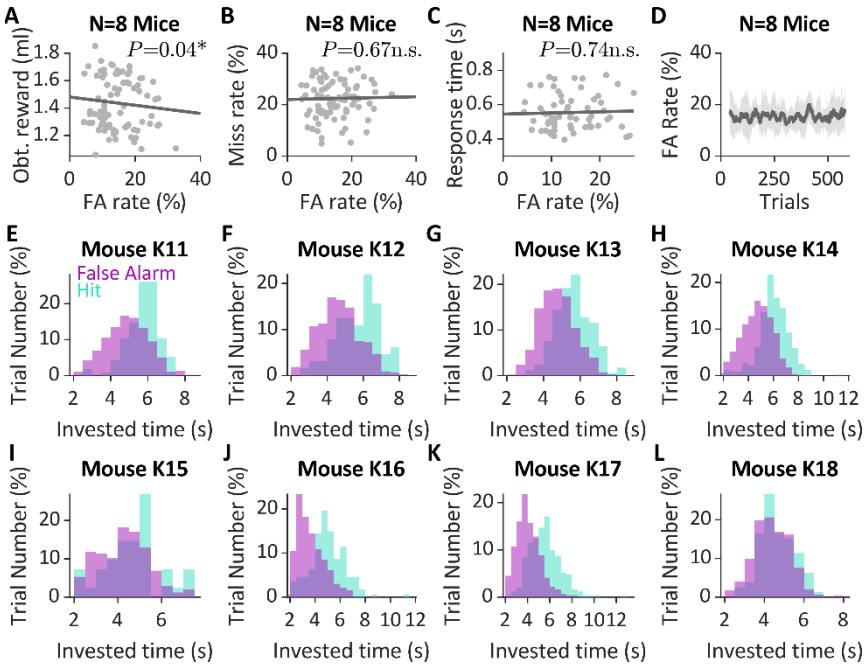

Fig. S4. HALIPs are not explained by non-perceptual factors. (A) Simple reward maximizing strategies do not explain false alarms. As expected from the task design, increasing false alarm rates result in decreased overall reward. Each dot indicates data from one session, line and p-value are from a least-square-fitted regression. (B-D) General task engagement does not account for false alarms. False alarm rates are related neither to miss rates on signal trials (B), nor to the time mice took to complete their response (C). (D) Fatigue or satiation does not readily explain false alarms. False alarm rates did not substantially increase or decrease over the course of a behavioral session. Plotted is the running mean false alarm rate [mean ± SD across animals, window 20 trials]. (E-L). Decision uncertainty or ambivalence does not explain high-confident false alarms. Time-investment-based confidence reports after false alarms and hits are overlapping in all mice, indicating that the false alarms with the largest time investments were perceived with comparable confidence as ‘true’ signals, and therefore likely reflected high-confidence faulty percepts, i.e., HALIPs.

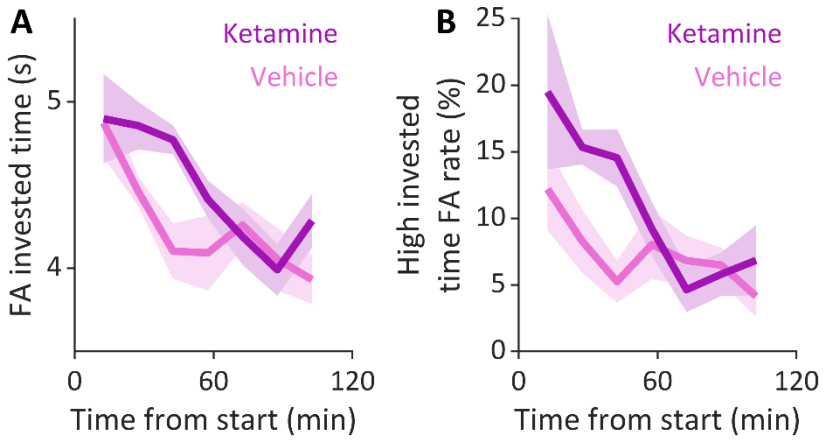

Fig. S5. Effect of ketamine on HALIPs is transient. Time-investment based confidence in false alarms and high-confidence false alarm rate [mean ± SD across mice] are increased in the first hour after ketamine administration as compared to vehicle, but not later. This is consistent with the relatively short half-life of ketamine of ~45 minutes.

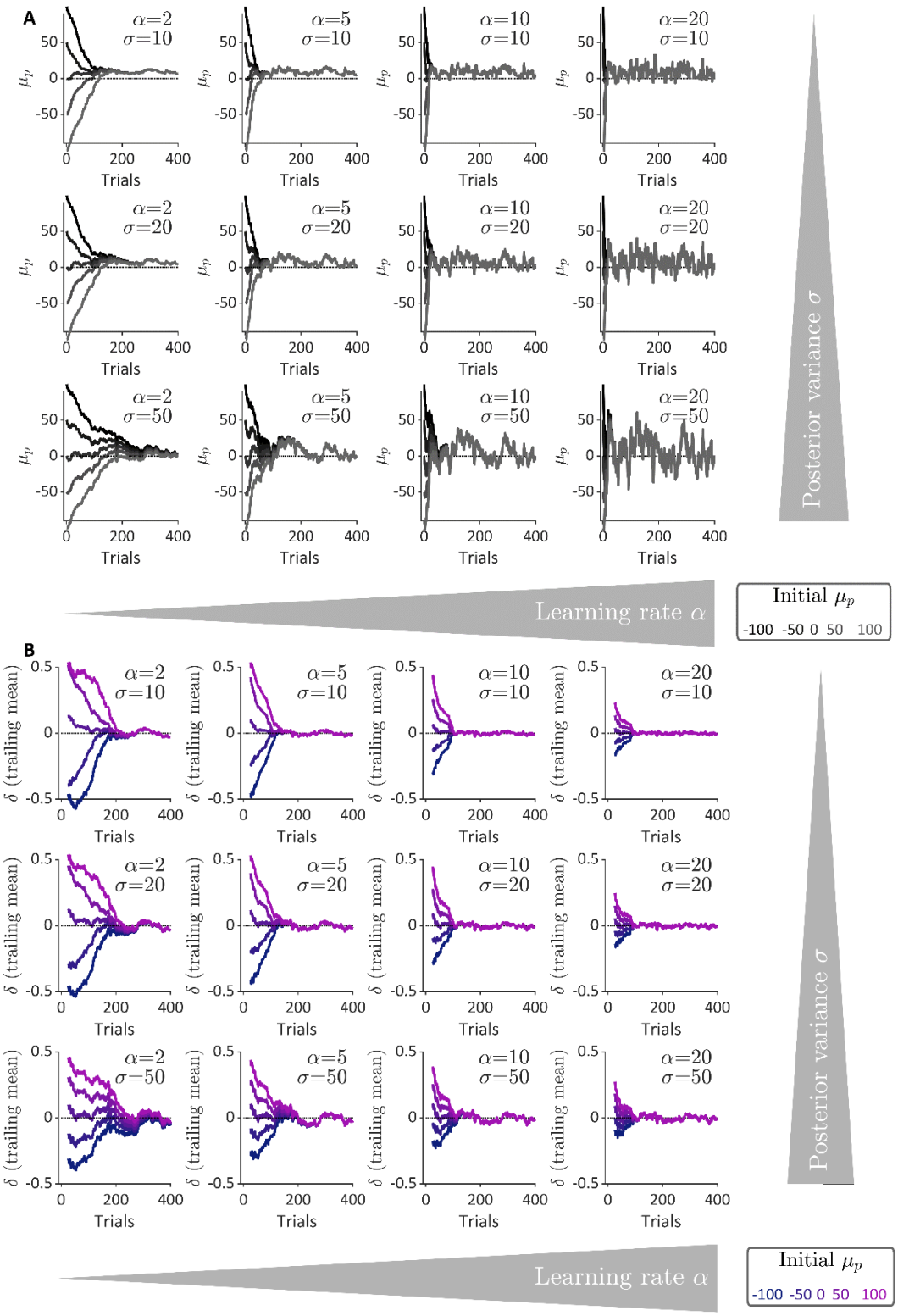

Fig. S6. Belief-udpating model learns to minimize surprise under different parameter settings. (A-B) The prior μ_p (A) converges to a stable level that minimizes perceptual prediction errors δ (B). This is observed for different values of the initial value for μ_p (colors), the learning rate α (columns), and posterior variance σ (rows). For visualization purposes, prediction errors δ are smoothed with trailing mean over a window of n=80 trials.

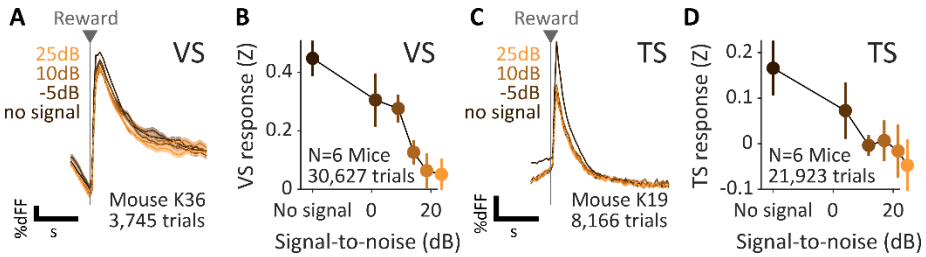

Fig. S7. Striatal dopamine shows phasic increases after rewarding outcomes. (A, C) Example dopamine signal time-series show phasic increase aligned to the delivery of water reward in both ventral striatum (A) and tail of striatum (C). (B, D) Response amplitudes [mean ± SD across mice] show decreasing responses with increasing stimulus signal-to-noise ratio. Note that only rewarded trials are included in these analyses.

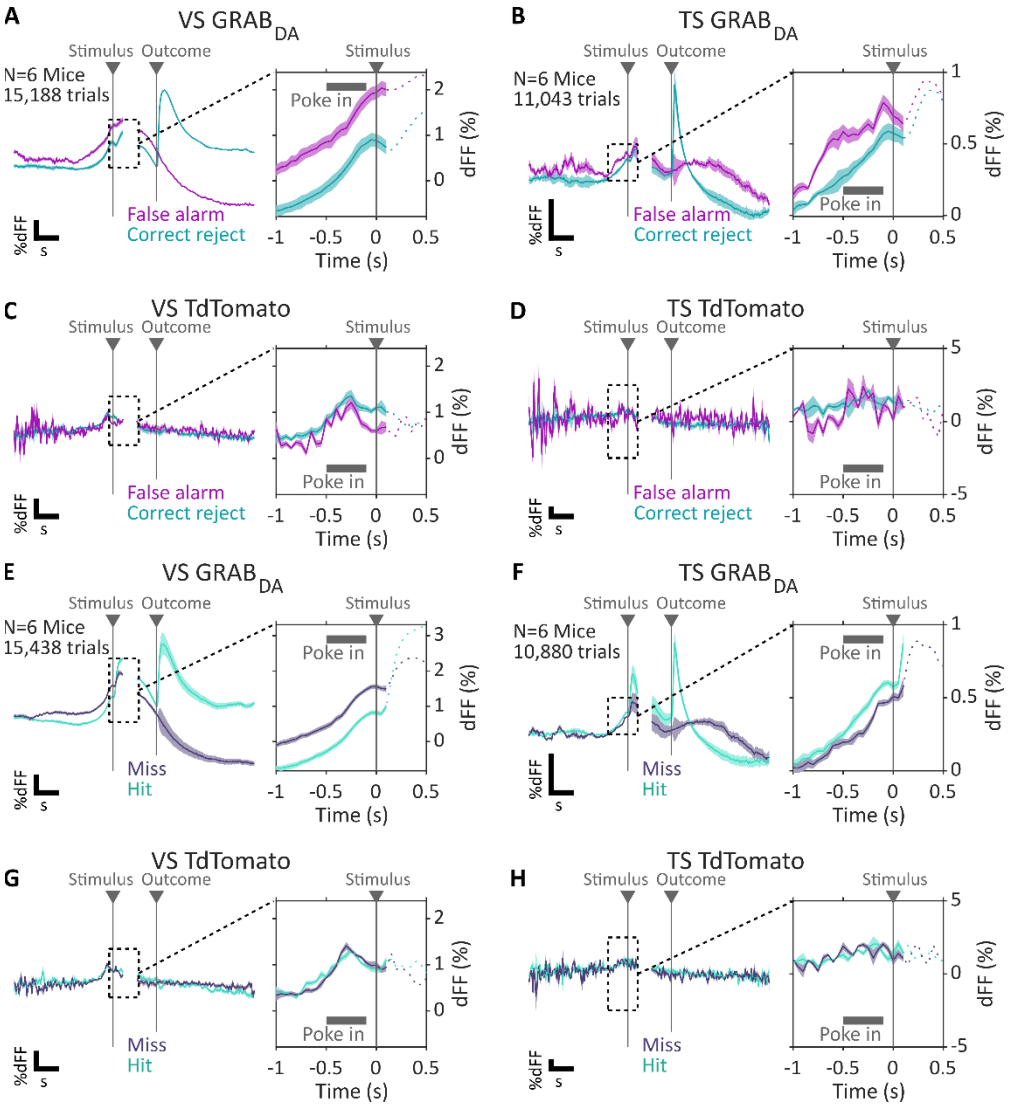

Fig. S8: Striatal dopamine signals are not explained by non-dopamine-related fluorescence fluctuations. (**A-B**) Fluorescence measured with the dopamine sensor GRAB$_{DA}$ on no-signal trials shows consistent tonic increases prior to false alarms as compared to correct rejections, as well as phasic responses to outcome delivery, both in ventral striatum (A) and tail of striatum (B) (**C-D**) Fluorescence measured with the dopamine-independent control fluorophore TdTomato neither shows consistent tonic increases prior to false alarms as compared to correct rejections, nor phasic responses after outcome delivery. (**E-F**) GRAB$_{DA}$ fluorescence on signal trials shows dissociation between ventral striatum (E) and tail of striatum in tonic increases prior to hits as compared to misses. (**G-H**) TdTomato fluorescence does not show any tonic increases prior to hits or misses. Lines and areas represent mean ± sem averaged across mice. Data are corrected for inter-individual variance by subtracting the subject mean and adding the grand mean at each time-point.

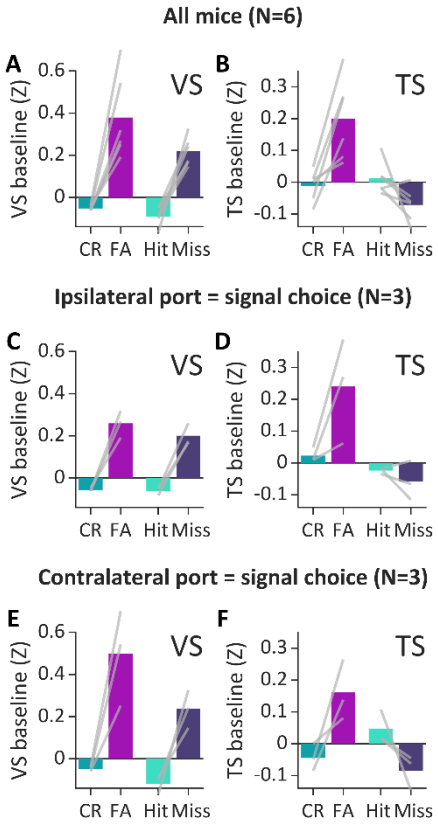

Fig. S9: Dissociation of tonic dopamine signals in VS and TS is not explained by differential involvement in movement preparation. (A-B) All mice show increased tonic dopamine activity prior to errors, i.e. false alarms (FA) and misses, in VS (A), and increased dopamine activity prior to signal choices, i.e. false alarms and hits, in TS (B). (C-D) This pattern is observed in mice that report a signal choice (false alarms and hits) with a movement to the side of the fiber location. (E-F) This pattern is equally observed in mice that report a signal choice with a movement away from the side of the fiber location show the same pattern.
Baseline dopamine is the signal integrated over a 0.5 s interval before the trial initiation poke, and z-scored within subject. Bar plots represent the mean across mice, gray lines represent single subjects. FA – false alarm, CR – correct reject.

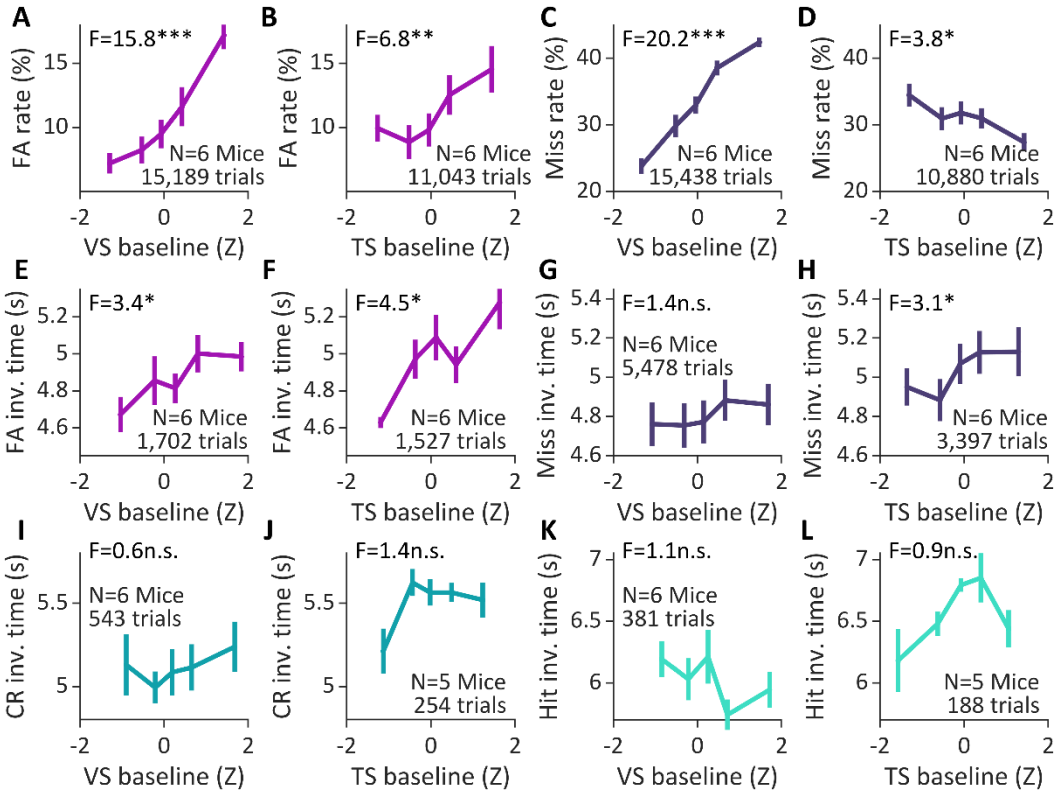

Fig. S10. Tonic dopamine signals are predictive of false alarm rate and false alarm confidence consistently across ventral (VS) and tail of striatum (TS). (A-B) On no-signal trials, increasing tonic baseline dopamine is associated with increasing false alarm rates in both VS (A) and TS (B). (C-D) On signal trials, increased tonic baseline dopamine predicts increased miss rates in the VS (C), but decreased miss rates (and therefore increased hit rates) in the TS (D). This is consistent with the idea that VS tonic dopamine encodes the probability of making an error choice (Fig. 5O), while TS tonic dopamine encodes the probability of making a signal choice (Fig. 5R). (E-F) On false alarm trials, increasing tonic baseline dopamine predicts increasing upcoming time investment-based confidence in both VS and TS. (G-L) On all other trials, the effects of baseline dopamine on time investments are weaker (H) or non-significant (G, I-L). This is in line with the idea that high levels of baseline DA at the beginning of a trial are needed to robustly virtualize an erroneous signal percept in the absence of a signal so that it is experienced with full confidence.

FA – false alarm, CR correct reject, inv. time – invested time

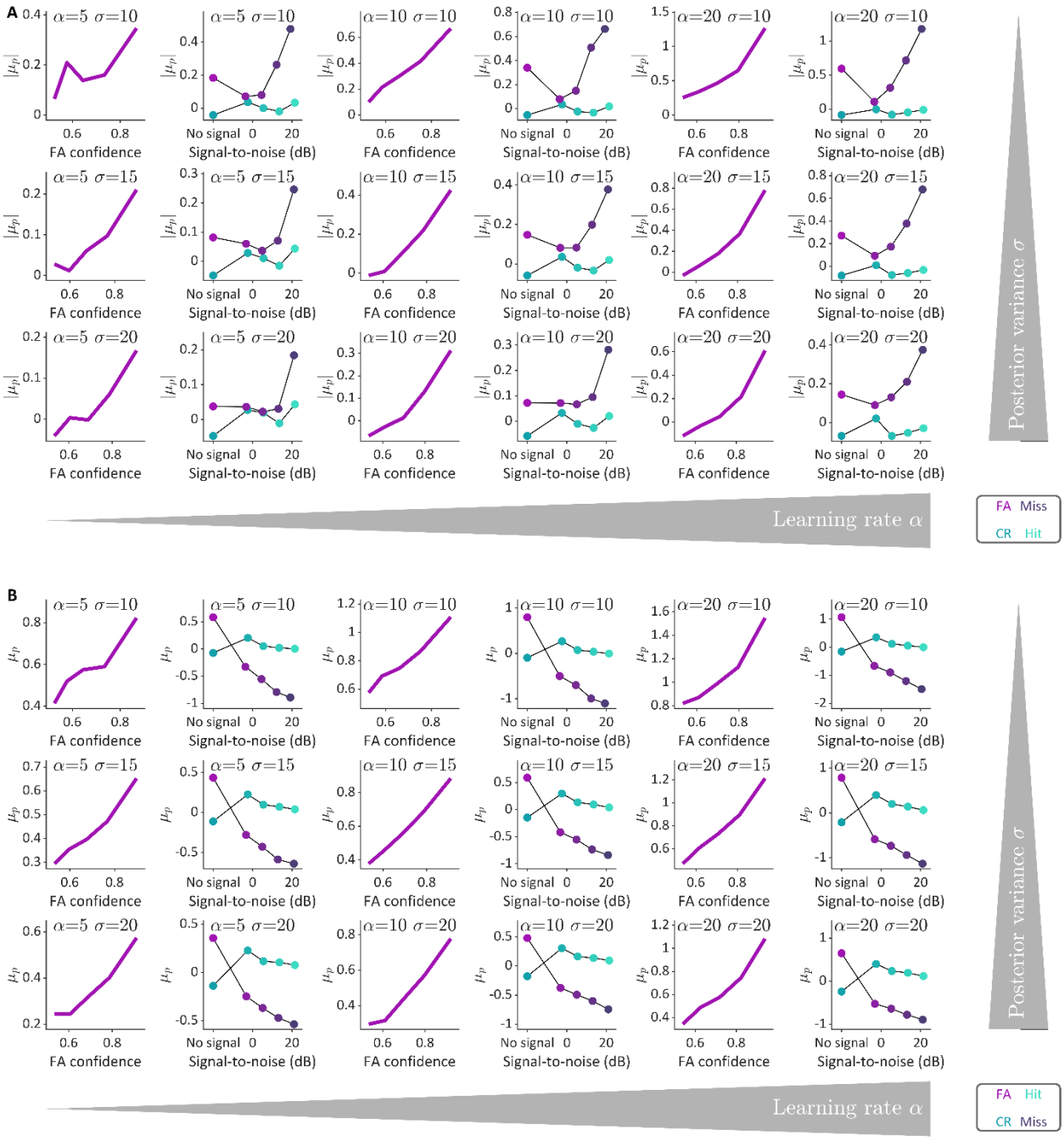

Fig. S11. Expectations from belief-updating model account for HALIPs under different parameter settings. (A) Reward expectations ($|\mu_P|$) behave like tonic dopamine in VS across different learning rates α (columns) and posterior variance σ (rows) values. On no-signal trials, $|\mu_P|$ is related to HALIPs (high-confidence in false alarms). This is because $|\mu_P|$ is generally increased on error choices, thereby recapitulating tonic DA signals in VS. (**B**) Signal expectations (μ_P) behave like tonic dopamine in TS across different parameter across different parameter settings. μ_P is related to HALIPs, and generally increased on signal choices, thereby recapitulating tonic DA signals in TS.

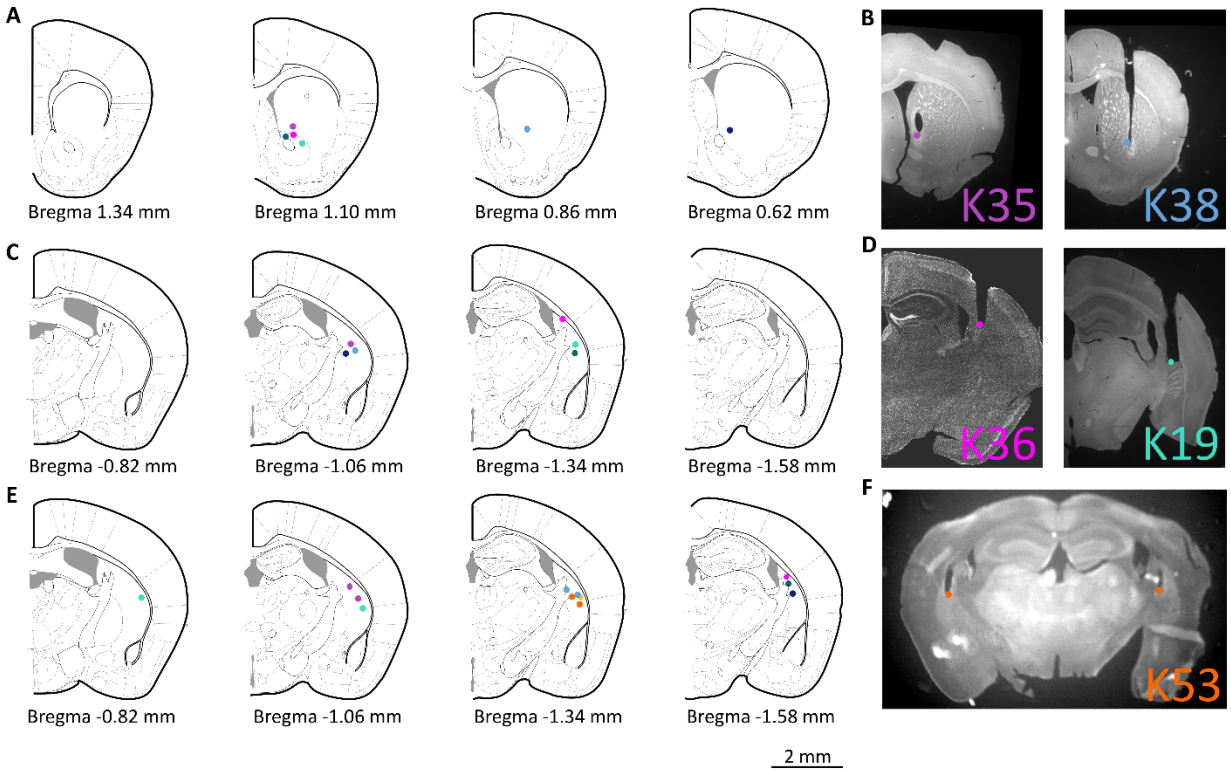

Fig. S12. Fiber implantation sites for photometry and optogenetics experiments. (A-D) Location of optic fibers used to collect $GRAB_{DA}$ fluorescence for measuring dopamine in ventral striatum (A) and the tail of striatum (B, Fig. 5). (E-F) Location of optic fibers used for laser stimulation in DAT-Ai32 mice in tail of striatum (Fig. 6). (A, C, E) Schematic summary of fiber implantation sites. Each dot represents one fiber site, each color represents one animal. Two dots of the same color represent bilateral fiber implantation. (B, D, F) Examples of fiber implantation sites.

Experiment	Figure	Age (weeks)
Behavior	Fig. 1	15 - 31
Expectations	Fig. 2A-H	32 - 36
Ketamine	Fig. 2I-O	36 - 50
Photometry	Fig. 5	26 - 46
Optogenetics	Fig. 6B-H	18 - 48
Haloperidol Rescue	Fig. 6I-J	21 - 27

Table S1. Age ranges of mice used for different experiments.

	Distribution	Hallucinations (CAPS score)	P-value
Age	35, 18-81 [median, range]	R=-0.11	0.10
Gender	127 - 93 [female - male]	59.7±5.1 - 55.5±5.5	0.58
Handedness	194 - 26 [right - left]	57.9±4.0 - 57.7±10.8	0.98
Smoker	161 - 59 [no - yes]	50.7±4.1 - 77.7±8.0	<0.001**
Coffee	55 - 165 [no - yes]	50.7±7.7 - 60.3±4.3	0.27
Education	55 - 131 - 34 [high school - college - graduate]	63.9±7.7 - 61.9±5.0 - 33.1±7.1	0.02*

Table S2. Demographic information and relationship to self-reported hallucination proneness for human participants. Self-reported hallucination proneness quantified by the Cardiff Anomalous Perception Scale (CAPS) in our non-clinical sample is significantly related to smoking status and to lower education levels. Both these demographic factors are known to be associated with psychotic disorders. For the continuous variable 'Age', the Spearman correlation coefficient with 'Hallucinations' is given. For all other categorical variables, the 'Hallucinations' values [mean ± sem] are given for each category and P-values are for the category main effect in ANOVA.

Data S1. Behavioral Data and MATLAB code to run analyses and generate plots. Data are saved in MATLAB mat-files ‘mouseData.mat’ and ‘humanData.mat’. The MATLAB m-file ‘StartHere.m’ performs analyses, saves results and generates plots. A more detailed description of the data format and the analysis code can be found in txt-file ‘ReadMe.txt’.

References

1. A. Carlsson, M. Lindqvist, Effect of Chlorpromazine or Haloperidol on Formation of 3-Methoxytyramine and Normetanephrine in Mouse Brain. *Acta Pharmacol. Toxicol.* **20**, 140–144 (1963). doi:10.1111/j.1600-0773.1963.tb01730.x Medline

2. B. Angrist, G. Sathananthan, S. Wilk, S. Gershon, Amphetamine psychosis: Behavioral and biochemical aspects. *J. Psychiatr. Res.* **11**, 13–23 (1974). doi:10.1016/0022-3956(74)90064-8 Medline

3. M. Laruelle, A. Abi-Dargham, Dopamine as the wind of the psychotic fire: New evidence from brain imaging studies. *J. Psychopharmacol.* **13**, 358–371 (1999). doi:10.1177/026988119901300405 Medline

4. J. Reith, C. Benkelfat, A. Sherwin, Y. Yasuhara, H. Kuwabara, F. Andermann, S. Bachneff, P. Cumming, M. Diksic, S. E. Dyve, P. Etienne, A. C. Evans, S. Lal, M. Shevell, G. Savard, D. F. Wong, G. Chouinard, A. Gjedde, Elevated dopa decarboxylase activity in living brain of patients with psychosis. *Proc. Natl. Acad. Sci. U.S.A.* **91**, 11651–11654 (1994). doi:10.1073/pnas.91.24.11651 Medline

5. O. D. Howes, J. Kambeitz, E. Kim, D. Stahl, M. Slifstein, A. Abi-Dargham, S. Kapur, The nature of dopamine dysfunction in schizophrenia and what this means for treatment. *Arch. Gen. Psychiatry* **69**, 776–786 (2012). doi:10.1001/archgenpsychiatry.2012.169 Medline

6. N. R. Swerdlow, M. Weber, Y. Qu, G. A. Light, D. L. Braff, Realistic expectations of prepulse inhibition in translational models for schizophrenia research. *Psychopharmacology* **199**, 331–388 (2008). doi:10.1007/s00213-008-1072-4 Medline

7. A. R. Powers, C. Mathys, P. R. Corlett, Pavlovian conditioning–induced hallucinations result from overweighting of perceptual priors. *Science* **357**, 596–600 (2017). doi:10.1126/science.aan3458 Medline

8. C. M. Cassidy, P. D. Balsam, J. J. Weinstein, R. J. Rosengard, M. Slifstein, N. D. Daw, A. Abi-Dargham, G. Horga, A Perceptual Inference Mechanism for Hallucinations Linked to Striatal Dopamine. *Curr. Biol.* **28**, 503–514.e4 (2018). doi:10.1016/j.cub.2017.12.059 Medline

9. M. Carandini, A. K. Churchland, Probing perceptual decisions in rodents. *Nat. Neurosci.* **16**, 824–831 (2013). doi:10.1038/nn.3410 Medline

10. A. Kepecs, N. Uchida, H. A. Zariwala, Z. F. Mainen, Neural correlates, computation and behavioural impact of decision confidence. *Nature* **455**, 227–231 (2008). doi:10.1038/nature07200 Medline

11. A. Lak, G. M. Costa, E. Romberg, A. A. Koulakov, Z. F. Mainen, A. Kepecs, Orbitofrontal cortex is required for optimal waiting based on decision confidence. *Neuron* **84**, 190–201 (2014). doi:10.1016/j.neuron.2014.08.039 Medline

12. P. Masset, T. Ott, A. Lak, J. Hirokawa, A. Kepecs, Behavior- and Modality-General Representation of Confidence in Orbitofrontal Cortex. *Cell* **182**, 112–126.e18 (2020). doi:10.1016/j.cell.2020.05.022 Medline

13. B. Hangya, J. I. Sanders, A. Kepecs, A Mathematical Framework for Statistical Decision Confidence. *Neural Comput.* **28**, 1840–1858 (2016). doi:10.1162/NECO_a_00864 Medline

14. See supplementary materials.

15. P. R. Corlett, G. Horga, P. C. Fletcher, B. Alderson-Day, K. Schmack, A. R. Powers, Hallucinations and Strong Priors. *Trends Cognit. Sci.* **23**, 114–127 (2019). doi:10.1016/j.tics.2018.12.001

16. J. H. Krystal, L. P. Karper, J. P. Seibyl, G. K. Freeman, R. Delaney, J. D. Bremner, G. R. Heninger, M. B. Bowers Jr., D. S. Charney, Subanesthetic effects of the noncompetitive NMDA antagonist, ketamine, in humans. Psychotomimetic, perceptual, cognitive, and neuroendocrine responses. *Arch. Gen. Psychiatry* **51**, 199–214 (1994). doi:10.1001/archpsyc.1994.03950030035004 Medline

17. V. Bell, P. W. Halligan, H. D. Ellis, The Cardiff Anomalous Perceptions Scale (CAPS): A new validated measure of anomalous perceptual experience. *Schizophr. Bull.* **32**, 366–377 (2006). doi:10.1093/schbul/sbj014 Medline

18. Pearson Symptom Checklist-90-Revised; www.pearsonclinical.com/psychology/products/100000645/symptom-checklist-90-revised-scl90r.html.

19. J. van Os, R. J. Linscott, I. Myin-Germeys, P. Delespaul, L. Krabbendam, A systematic review and meta-analysis of the psychosis continuum: Evidence for a psychosis proneness-persistence-impairment model of psychotic disorder. *Psychol. Med.* **39**, 179–195 (2009). doi:10.1017/S0033291708003814 Medline

20. A. Lak, E. Hueske, J. Hirokawa, P. Masset, T. Ott, A. E. Urai, T. H. Donner, M. Carandini, S. Tonegawa, N. Uchida, A. Kepecs, Reinforcement biases subsequent perceptual decisions when confidence is low, a widespread behavioral phenomenon. *eLife* **9**, e49834 (2020). doi:10.7554/eLife.49834 Medline

21. W. Schultz, P. Dayan, P. R. Montague, A neural substrate of prediction and reward. *Science* **275**, 1593–1599 (1997). doi:10.1126/science.275.5306.1593 Medline

22. Q. Xiong, P. Znamenskiy, A. M. Zador, Selective corticostriatal plasticity during acquisition of an auditory discrimination task. *Nature* **521**, 348–351 (2015). doi:10.1038/nature14225 Medline

23. W. Menegas, K. Akiti, R. Amo, N. Uchida, M. Watabe-Uchida, Dopamine neurons projecting to the posterior striatum reinforce avoidance of threatening stimuli. *Nat. Neurosci.* **21**, 1421–1430 (2018). doi:10.1038/s41593-018-0222-1 Medline

24. F. Sun, J. Zeng, M. Jing, J. Zhou, J. Feng, S. F. Owen, Y. Luo, F. Li, H. Wang, T. Yamaguchi, Z. Yong, Y. Gao, W. Peng, L. Wang, S. Zhang, J. Du, D. Lin, M. Xu, A. C. Kreitzer, G. Cui, Y. Li, A genetically-encoded fluorescent sensor enables rapid and specific detection of dopamine in flies, fish, and mice. *Cell* **174**, 481–496.e19 (2018). doi:10.1016/j.cell.2018.06.042 Medline

25. T. Sigurdsson, K. L. Stark, M. Karayiorgou, J. A. Gogos, J. A. Gordon, Impaired hippocampal-prefrontal synchrony in a genetic mouse model of schizophrenia. *Nature* **464**, 763–767 (2010). doi:10.1038/nature08855 Medline

26. S. Parnaudeau, P. K. O'Neill, S. S. Bolkan, R. D. Ward, A. I. Abbas, B. L. Roth, P. D. Balsam, J. A. Gordon, C. Kellendonk, Inhibition of mediodorsal thalamus disrupts thalamofrontal connectivity and cognition. *Neuron* **77**, 1151–1162 (2013). doi:10.1016/j.neuron.2013.01.038 Medline

27. J. J. Weinstein, M. O. Chohan, M. Slifstein, L. S. Kegeles, H. Moore, A. Abi-Dargham, Pathway-Specific Dopamine Abnormalities in Schizophrenia. *Biol. Psychiatry* **81**, 31–42 (2017). doi:10.1016/j.biopsych.2016.03.2104 Medline

28. S. Kapur, Psychosis as a state of aberrant salience: A framework linking biology, phenomenology, and pharmacology in schizophrenia. *Am. J. Psychiatry* **160**, 13–23 (2003). doi:10.1176/appi.ajp.160.1.13 Medline

29. A. Heinz, Dopaminergic dysfunction in alcoholism and schizophrenia—Psychopathological and behavioral correlates. *Eur. Psychiatry* **17**, 9–16 (2002). doi:10.1016/S0924-9338(02)00628-4 Medline

30. N. R. Swerdlow, G. F. Koob, Dopamine, schizophrenia, mania, and depression: Toward a unified hypothesis of cortico-striatopallido-thalamic function. *Behav. Brain Sci.* **10**, 197–208 (1987). doi:10.1017/S0140525X00047488

31. D. R. Hemsley, J. N. P. Rawlins, J. Feldon, S. H. Jones, J. A. Gray, The neuropsychology of schizophrenia: Act 3. *Behav. Brain Sci.* **16**, 209–215 (1993). doi:10.1017/S0140525X00029708

32. R. A. Adams, K. E. Stephan, H. R. Brown, C. D. Frith, K. J. Friston, The computational anatomy of psychosis. *Front. Psychiatry* **4**, 47 (2013). doi:10.3389/fpsyt.2013.00047 Medline

33. A. Lak, K. Nomoto, M. Keramati, M. Sakagami, A. Kepecs, Midbrain Dopamine Neurons Signal Belief in Choice Accuracy during a Perceptual Decision. *Curr. Biol.* **27**, 821–832 (2017). doi:10.1016/j.cub.2017.02.026 Medline

34. W. Menegas, B. M. Babayan, N. Uchida, M. Watabe-Uchida, Opposite initialization to novel cues in dopamine signaling in ventral and posterior striatum in mice. *eLife* **6**, e21886 (2017). doi:10.7554/eLife.21886 Medline

35. N. D. Ponvert, S. Jaramillo, Auditory Thalamostriatal and Corticostriatal Pathways Convey Complementary Information about Sound Features. *J. Neurosci.* **39**, 271–280 (2019). doi:10.1523/JNEUROSCI.1188-18.2018 Medline

36. P. Znamenskiy, A. M. Zador, Corticostriatal neurons in auditory cortex drive decisions during auditory discrimination. *Nature* **497**, 482–485 (2013). doi:10.1038/nature12077 Medline

37. G. Horga, A. Abi-Dargham, An integrative framework for perceptual disturbances in psychosis. *Nat. Rev. Neurosci.* **20**, 763–778 (2019). doi:10.1038/s41583-019-0234-1 Medline

38. B. J. Hunnicutt, B. C. Jongbloets, W. T. Birdsong, K. J. Gertz, H. Zhong, T. Mao, A comprehensive excitatory input map of the striatum reveals novel functional organization. *eLife* **5**, e19103 (2016). doi:10.7554/eLife.19103 Medline

39. S. Soares, B. V. Atallah, J. J. Paton, Midbrain dopamine neurons control judgment of time. *Science* **354**, 1273–1277 (2016). doi:10.1126/science.aah5234 Medline

40. B. O'Neill, J. C. Patel, M. E. Rice, Characterization of Optically and Electrically Evoked Dopamine Release in Striatal Slices from Digenic Knock-in Mice with DAT-Driven Expression of Channelrhodopsin. *ACS Chem. Neurosci.* **8**, 310–319 (2017). doi:10.1021/acschemneuro.6b00300 Medline

41. L. T. Coddington, J. T. Dudman, The timing of action determines reward prediction signals in identified midbrain dopamine neurons. *Nat. Neurosci.* **21**, 1563–1573 (2018). doi:10.1038/s41593-018-0245-7 Medline